

**DANISH METEOROLOGICAL INSTITUTE**

**—— SCIENTIFIC REPORT ——**

**00-17**

**Structure Function Characteristics for  
2 meter Temperature and Relative Humidity  
in Different Horizontal Resolutions**

**Kai Sattler**

**Xiang-Yu Huang**



**COPENHAGEN 2000**

**ISSN-Nr. 0905-3263 (printed)**  
**ISSN Nr. 1399-1949 (online)**  
**ISBN-Nr. 87-7478-428-5**

# Structure Function Characteristics for 2 meter Temperature and Relative Humidity in Different Horizontal Resolutions

## Abstract

The isotropic correlations of forecast errors in the HIRLAM system are investigated for different horizontal grid sizes in order to achieve an improved representation of the structure functions for high resolution surface analysis. The investigation is performed for 2 meter temperature and relative humidity and makes use of operational forecasts from DMI-HIRLAM at DMI, which can support the background for a surface analysis in three different horizontal resolutions. Two different well known methods for determining isotropic forecast error correlations are applied. The first method compares forecasts to observations (Hollingsworth–Lönnberg Method), while the second makes use of two different forecasts valid for the same time (NMC–Method). The latter method is also used to investigate isotropy as well as the influence of land–sea contrast and orography. A comparison of the two mentioned methods reveals a good correspondence between them, and the investigation of monthly changes reveals some seasonal tendencies. A further comparison with the structure functions currently used in the surface analysis scheme of HIRLAM gives some hints on their applicability in the context of the different model resolutions of DMI-HIRLAM. The results suggest a decrease in the background error correlation scales when going to higher horizontal resolution in the forecast model.

## Contents

|          |   |           |
|----------|---|-----------|
| <b>1</b> | <b>Introduction</b>   | <b>3</b>  |
| <b>2</b> | <b>Structure function determination</b>                       | <b>5</b>  |
| 2.1      | Hollingsworth–Lönnerberg Method . . . . .                     | 5         |
| 2.2      | NMC Method . . . . .  | 6         |
| 2.3      | Quality Control . . . . .                                     | 7         |
| 2.4      | Consistency . . . . .   | 7         |
| <b>3</b> | <b>Structure functions in DMI-HIRLAM</b>                      | <b>9</b>  |
| 3.1      | General . . . . .   | 9         |
| 3.2      | Quality Control Limits . . . . .                              | 11        |
| 3.3      | Correlation fields . . . . .                                  | 12        |
| 3.4      | Isotropic correlation curves . . . . .                        | 15        |
| 3.4.1    | Surface dependencies . . . . .                                | 16        |
| 3.4.2    | Comparison and monthly changes . . . . .                      | 19        |
| 3.4.3    | Scale estimations . . . . .                                   | 23        |
| <b>4</b> | <b>Comments on the current HIRLAM surface analysis scheme</b> | <b>25</b> |
| 4.1      | Error standard deviation . . . . .                            | 25        |
| 4.2      | Correlation scale . . . . .                                   | 26        |
| <b>5</b> | <b>Conclusions</b>  | <b>27</b> |
| <b>A</b> | <b>List of Symbols</b>  | <b>28</b> |
|          | <b>References</b>   | <b>29</b> |

## 1 Introduction

During recent years, the trend towards high resolution weather forecasting has continued. Connected to this has been the development of analysis schemes for temperature, humidity, wind and other parameters at near surface levels (Navascues 1997) as well as in the mesoscale (Häggmark et al. 2000). These schemes are based on optimum interpolation (Gandin 1963) and, apart from they are univariate and 2-dimensional (horizontal), are similar to the analysis schemes that have been used for upper level parameters in many operational numerical weather prediction systems (Lorenc 1981).

Within the calculation of the analysis increment using OI, the statistical structure functions play a major role. Each function represents the spatial background error covariances of a certain variable (Hollingsworth and Lönnberg 1986). These covariances are assumed to be isotropic and homogeneous in order to simplify the analysis (Daley 1991). One way to estimate the background error covariances is to use both background and observations, as proposed by Hollingsworth and Lönnberg (1986) and Lönnberg and Hollingsworth (1986). The method is often referred to as Hollingsworth–Lönnberg Method and has been used for years. With the Hollingsworth–Lönnberg Method, the determination of the structure functions needs a reliable observation network which is homogeneous over a long period of time. An alternative to Hollingsworth–Lönnberg Method, that also goes back to Lönnberg and Hollingsworth (1986), is the exclusive use of background data when evaluating the structure functions (Parrish and Derber 1992). The method is often referred to as NMC–Method and is based on the assumption that the forecast errors grow linearly with time. The NMC–Method has been successfully applied in recent years [e. g. Parrish and Derber 1992, Rabier et al. 1998]. Since both methods require a homogeneous series of forecasts, the structure functions need to be reevaluated as soon as the forecast model is changed at some major points (Puri and Lönnberg 1991).

A scheme for the analysis of 2 meter temperature (T2m) and relative humidity (RH2m) was developed within the international HIRLAM work by Navascues (1997). The structure functions used in the analysis scheme take care of land–sea contrast (Gustafsson 1985) and vertical displacements (Navascues 1997). This so-called surface analysis scheme of HIRLAM was applied at DMI during a research project concerned with T2m and RH2m analysis over Denmark for agricultural purposes (Sattler et al. 2000). The horizontal resolution was 5 km corresponding to the operational high resolution forecasting model for Denmark DMI-HIRLAM-D (Sass et al. 1999), which supported the background data. This resolution was remarkably higher than usually applied in the surface analysis scheme, where background fields of up to  $0.2^\circ$  horizontal resolution are used (Garçia–Moya et al. 2000 and Rodríguez 2000), and the results of Sattler et al. 2000 suggest a reevaluation of the structure functions for background data with such high a horizontal grid resolution.

In the following sections, the structure functions for T2m and RH2m are determined for the three operational models DMI-HIRLAM-G, DMI-HIRLAM-E and DMI-HIRLAM-D. These three models are arranged in a triply nested mode, with horizontal resolutions of  $\approx 45$  km, 15 km and 5 km respectively. Details are given by Sass et al. (1999).

Two different methods for determining a correlation of forecast errors between different locations

within the forecasting model domain are utilized: The Hollingsworth–Lönnerberg Method and the NMC–Method, which are mentioned above. They are described in short in the sections 2.1 and 2.2. Further considerations for the application of the methods are outlined in sections 2.3 and 2.4. Section 3 describes the application of the two mentioned methods. Section 4 shortly refers the results to the current HIRLAM surface analysis system. Some conclusions are drawn in section 5.

## 2 Structure function determination

### 2.1 Hollingsworth–Lönnberg Method

Within this method, the spatial structure of the background and observation error correlation is investigated in order to derive an isotropic correlation function. The method was first applied by Hollingsworth and Lönnberg (1986) and Lönnberg and Hollingsworth (1986). It determines a distance dependent structure function for the correlation of the difference between background and observation by building correlations between all available observation points. The background data usually refers to 6 hour forecasts, and the background error covariance between two points  $i$  and  $j$  is defined as

$$b_{ij}^{6h} = \left\langle \left( x_i^{b6} - x_i^t \right) \left( x_j^{b6} - x_j^t \right) \right\rangle, \quad (1)$$

where the pointed brackets denote the expectation value. Refer to the list of symbols for a description of the variables. The observation error covariance is analogously defined as

$$r_{ij} = \left\langle \left( x_i^r - x_i^t \right) \left( x_j^r - x_j^t \right) \right\rangle. \quad (2)$$

If we assume that there is no correlation between observation errors and background errors when regarding two different arbitrarily chosen points, then the sum of equation (1) and (2) leads to

$$s_{ij} = b_{ij}^{6h} + r_{ij} = \left\langle \left( x_i^{b6} - x_i^r \right) \left( x_j^{b6} - x_j^r \right) \right\rangle. \quad (3)$$

The sum of the covariances can be determined from available observation data and the respective model fields without knowing the true values  $x^t$ . By introducing a normalization using the auto-correlations as proposed by Daley (1991), we can determine a correlation of differences between background and observation for the two points  $i$  and  $j$ :

$$\frac{b_{ij}^{6h} + r_{ij}}{\sqrt{s_{ii}s_{jj}}}. \quad (4)$$

If we further assume that the observations at different sites are not correlated, then

$$r_{ij} = 0 \quad \text{for } i \neq j, \quad (5)$$

and equation 4 reduces to

$$c_{r,l}(i, j) = \frac{b_{ij}^{6h}}{\sqrt{s_{ii}s_{jj}}} \quad \text{for } i \neq j. \quad (6)$$

The correlation determined in this way still contains an uncertainty, which is due to a possible bias in the background fields. In order to reduce the influence of bias, the following correction is applied to the background data:

$$x_{corr}^{b6} = x^{b6} - \langle x^{b6} - x^r \rangle. \quad (7)$$

## 2.2 NMC Method

Errors, which occur within the running forecast model, propagate with a certain speed within the model domain. Thus, variables at a certain grid point become first influenced by errors from distant grid points after a certain amount of time. As a result, the correlation of two forecast fields, which are valid at the same time, but which refer to different forecast lengths, must include information about the state of propagation of such errors. The correlation of two such forecasts originating from the same model shows a spatial structure. This structure is similar to the correlations found with the Hollingsworth–Lönnerberg Method, and may be used to find error correlation scales (Parrish and Derber 1992). It can be regarded as isotropic as a first approximation.

The formulation for calculating the correlations is analogous to the Hollingsworth–Lönnerberg Method, but does not use observation data. The assumption of the Hollingsworth–Lönnerberg Method, that there is no correlation between observation errors and background errors, is not required by the NMC–Method.

Within this work, 36 hour forecasts and 12 hour forecasts started 24 hours later are used. The background error covariances for these two forecast lengths is

$$\begin{aligned} b_{ij}^{12h} &= \langle (x_i^{b12} - x_i^t) (x_j^{b12} - x_j^t) \rangle \\ b_{ij}^{36h} &= \langle (x_i^{b36} - x_i^t) (x_j^{b36} - x_j^t) \rangle. \end{aligned} \quad (8)$$

The sum of these covariances can be written as

$$b_{ij}^{12h} + b_{ij}^{36h} = \langle (x_i^{b12} - x_i^{b36}) (x_j^{b12} - x_j^{b36}) \rangle + \langle (x_i^{b12} - x_i^t) (x_j^{b36} - x_j^t) \rangle + \langle (x_j^{b12} - x_j^t) (x_i^{b36} - x_i^t) \rangle. \quad (9)$$

The first term on the right-hand side is what we can determine from the forecast data, namely the covariance between the background differences. It is the analogue to the term on the right-hand side of equation (3). Equation (9) actually states that the covariance we determine includes also covariances between background errors from two separated points with different forecast lengths.

If we now assume that the background errors behave linearly with respect to the forecast length, i. e.

$$\begin{aligned} x_i^{b12} - x_i^t &= \beta_i^{12} (x_i^{b6} - x_i^t) \\ x_i^{b36} - x_i^t &= \beta_i^{36} (x_i^{b6} - x_i^t), \end{aligned} \quad (10)$$

and if we further assume that the proportionality factors are constant, then it is possible to write from the equations (8) and (9) and using the 6 hour forecast error covariance:

$$\langle (x_i^{b12} - x_i^{b36}) (x_j^{b12} - x_j^{b36}) \rangle = \alpha b_{ij}^{6h} \quad (11)$$

With the introduction of a normalization like in the Hollingsworth–Lönnberg Method by using the autocorrelations, we finally get for the correlation from the NMC–Method:

$$c_{r,n}(i, j) = \frac{\langle (x_i^{b12} - x_i^{b36}) (x_j^{b12} - x_j^{b36}) \rangle}{\sqrt{\langle (x_i^{b12} - x_i^{b36})^2 \rangle \langle (x_j^{b12} - x_j^{b36})^2 \rangle}}. \quad (12)$$

A correction due to forecast bias is not necessary here, because both fields originate from the same forecast model.

### 2.3 Quality Control

When applying the Hollingsworth–Lönnberg Method, the results can be blurred when erroneous observations occur. It is therefore necessary to introduce a quality check in order to reject such data. With the simple assumption that the difference between background and observation must not exceed a given limit, we formulate

$$|x^{b6} - x^r| < \Delta x_{max}, \quad (13)$$

which at least ensures that gross errors are excluded.

### 2.4 Consistency

The correlation functions determined with the two above mentioned methods and described by equation (6) and (12) respectively, contain a significant difference in their characteristic behaviour, which becomes clear when regarding them at distance  $d = 0$  or  $i = j$ . While

$$\lim_{d \rightarrow 0} c_{r,n} = 1 \quad (14)$$

for the function from the NMC–Method (equation (12)), the limit for the function from the Hollingsworth–Lönnberg Method (equation (6)) is

$$\lim_{d \rightarrow 0} c_{r,l} = \frac{(\sigma_b)^2}{(\sigma_b)^2 + (\sigma_r)^2}, \quad (15)$$

because the observation errors are assumed to be spatially uncorrelated, so only the local errors contribute to the correlation (Daley 1991). This means that the correlation curve determined with the Hollingsworth–Lönnberg Method only includes correlations that are due to the background error.

In order to compare the structure functions determined with the two methods, a further normalization of  $c_{r,l}$  is necessary. It is possible to normalize  $c_{r,l}$  by using the limit from equation (15), so that  $c_{r,l} \rightarrow 1$  as  $d \rightarrow 0$ . However, this limit is not really known, because  $\sigma_r$  is unknown. It includes the random observation error, an instrument error and the uncertainty of representativeness of the observation. A quite useful estimation of the limit is possible though, if  $c_{r,l}$  is fitted to a representative function near  $d = 0$ . The intersection at  $d = 0$  then is a good approximation for the limit of equation (15).

It is assumed that the correlation curves behave in a way, where the first deviation with respect to  $d$  is steady and goes to zero at  $d = 0$ . A suitable function to fit the curves for small values of  $d$  is a Gaussian function:

$$c_{r,l}(d) = c_{r,l}(0) \exp\left(-\frac{d^2}{2L^2}\right) \quad \text{for } 0 \leq d \leq d_f. \quad (16)$$

The limit  $d_f$  for the fitting should be chosen such that it is large enough to cover the first points of  $c_{r,l}$ , that are represented in the respective model. The value of  $c_{r,l}(0)$  and  $L$  are determined during the fitting process. The further normalized curve of  $c_{r,l}$  then is:

$$c_{r,s}(d) = \frac{c_{r,l}(d)}{c_{r,l}(0)}. \quad (17)$$

$c_{r,s}$  is consistent with  $c_{r,n}$  and makes direct comparison possible.

### 3 Structure functions in DMI-HIRLAM

#### 3.1 General

The following investigations are separated into several parts. In the first part, the purpose is to find appropriate limits for the quality check in the application of the Hollingsworth–Lönnerberg Method. The bias correction is switched off during this part. We show the isotropic properties of the structure functions of DMI-HIRLAM background errors in the second part by looking at the horizontal correlations fields, making use of the NMC–Method. This also points out to a dependency of correlation from the land–sea distribution. The other parts are then concerned with the actual investigation of the isotropic structure functions in DMI-HIRLAM.

The structure function evaluations are performed with data from the three operational models DMI-HIRLAM-G, DMI-HIRLAM-E and DMI-HIRLAM-D. The model domains are shown in figure 1. The significant difference of their size may cause some uncertainties when comparing structure functions. However, it can be assumed that the forecast errors of 2 meter temperature and relative humidity are mainly influenced by changes of the surface properties like land–sea contrast, which has been taken into account by the models (see below). What the selection of observations is concerned, an equivalent set of observation sites is chosen for DMI-HIRLAM-G and DMI-HIRLAM-E. It contains 288 synoptic stations. The set used for DMI-HIRLAM-D includes a subset of 200 sites from these stations.

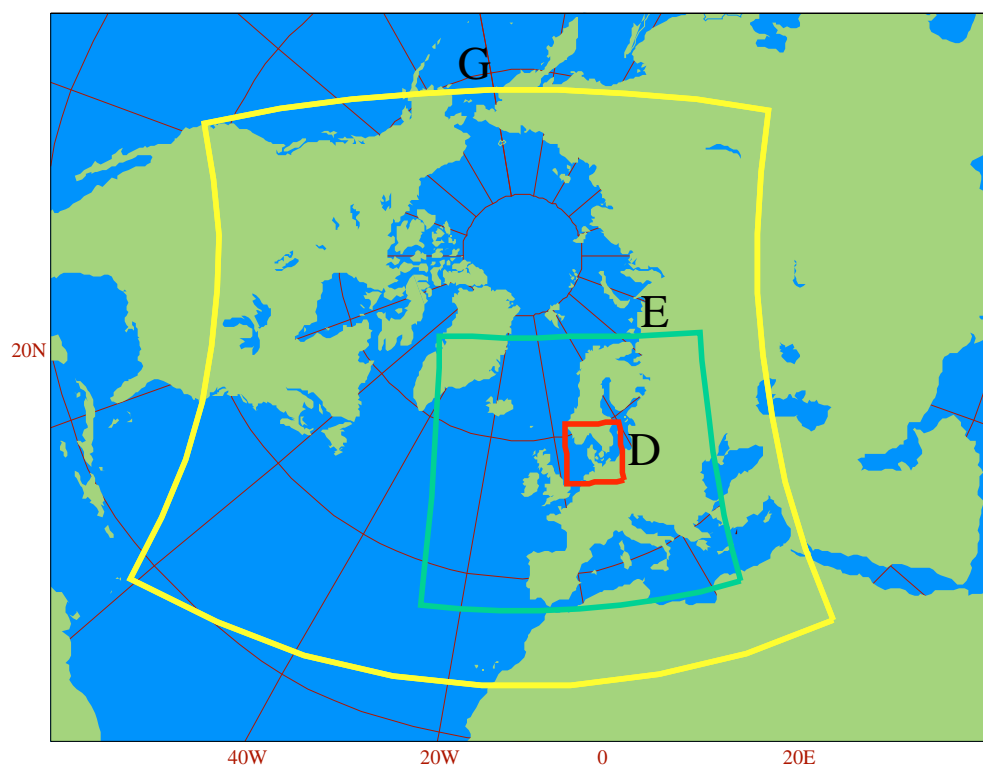


FIG. 1: Areas covered by the three operationally running models DMI-HIRLAM-G, DMI-HIRLAM-E and DMI-HIRLAM-D. The grid representation is in rotated geographic coordinates.

The Hollingsworth–Lönnerberg Method is applied as follows. Forecast fields based on analysis at 00 UTC and 12 UTC and valid 6 hours later are compared to synoptic observations from 06 UTC and 18 UTC respectively. The correlated differences are then referred to the distance between the respective sites. In addition to the mentioned quality control, a control of sample size is applied to reject those samples, which have sample size below 10 per month, before the correlation determination.

The NMC–Method is applied to the 12 hour forecast based on 00 UTC analysis and the respective 36 hour forecast from the day before. The correlations are determined for selected pairs of grid points and referred to the respective real distance between them.

The calculated correlations are not shown itself, but empirically averaged correlations for the selected separation intervals (Hollingsworth and Lönnerberg 1986). As the correlation samples are large and include at least several hundred elements per averaging interval, arithmetic averaging seems appropriate.

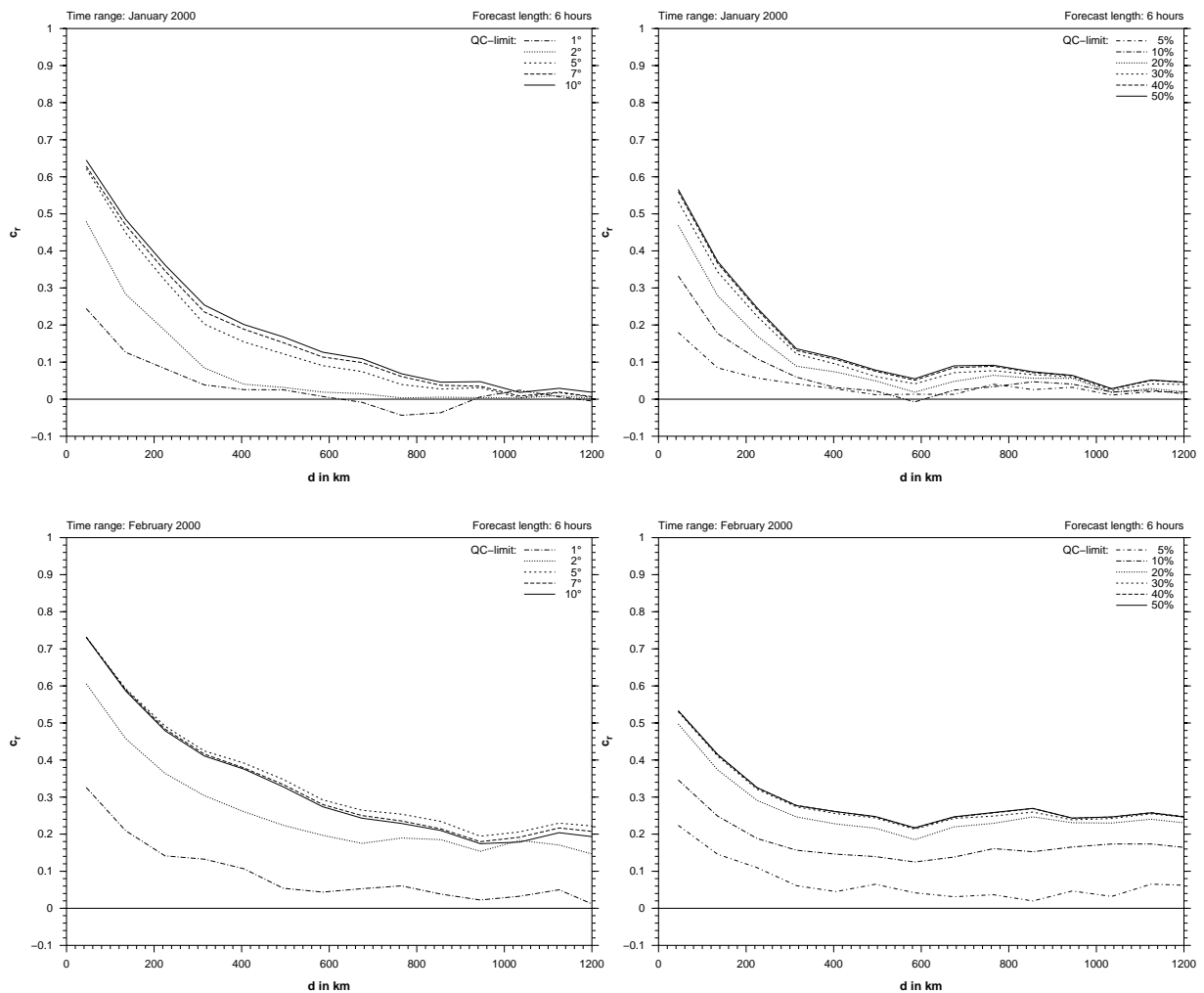


FIG. 2: Correlation of background minus observation in DMI-HIRLAM-G for T2m (left) and RH2m (right), valid for January (upper) and February (lower) respectively. The correlations are determined with 6 different quality control limits.

### 3.2 Quality Control Limits

As outlined in section 2.3, a quality check of the observations is applied, but the quality control limit  $\Delta x_{max}$  is still to be determined.

The limits for rejecting observation data are determined for both 2 meter temperature (T2m) and relative humidity (RH2m). Data from January and February 2000 are examined. We assume that the results are generally valid. Figure 2 shows correlation curves for the low resolution model DMI-HIRLAM-G. As no bias correction was applied in these calculations yet, the curves from February show high correlation values even for large distances. However, the effect from applying different limits in the quality control can be clearly recognized for both months. The same is valid for DMI-HIRLAM-E and DMI-HIRLAM-D (figures 3 and 4).

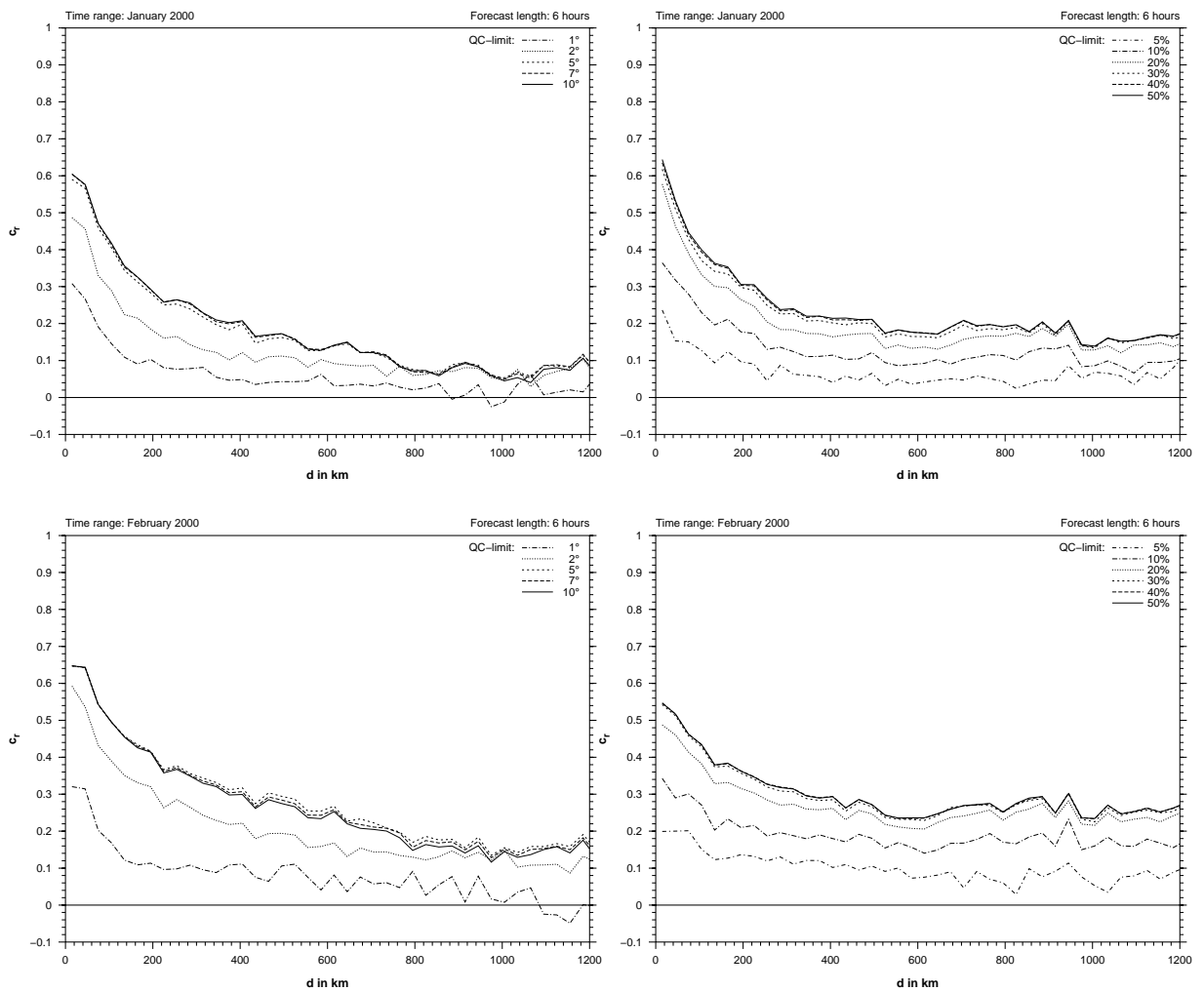


FIG. 3: Correlation of background minus observation in DMI-HIRLAM-E for T2m (left) and RH2m (right), valid for January (upper) and February (lower) respectively. The correlations are determined with 6 different quality control limits.

The correlation in T2m for DMI-HIRLAM-G drops remarkably for those differences which are below 5 K. The curves from February even indicate the vanishing influence of the bias (figure 2 lower left). Thus, the largest contribution to the bias seems to be due to errors within the range of 1–2 K.

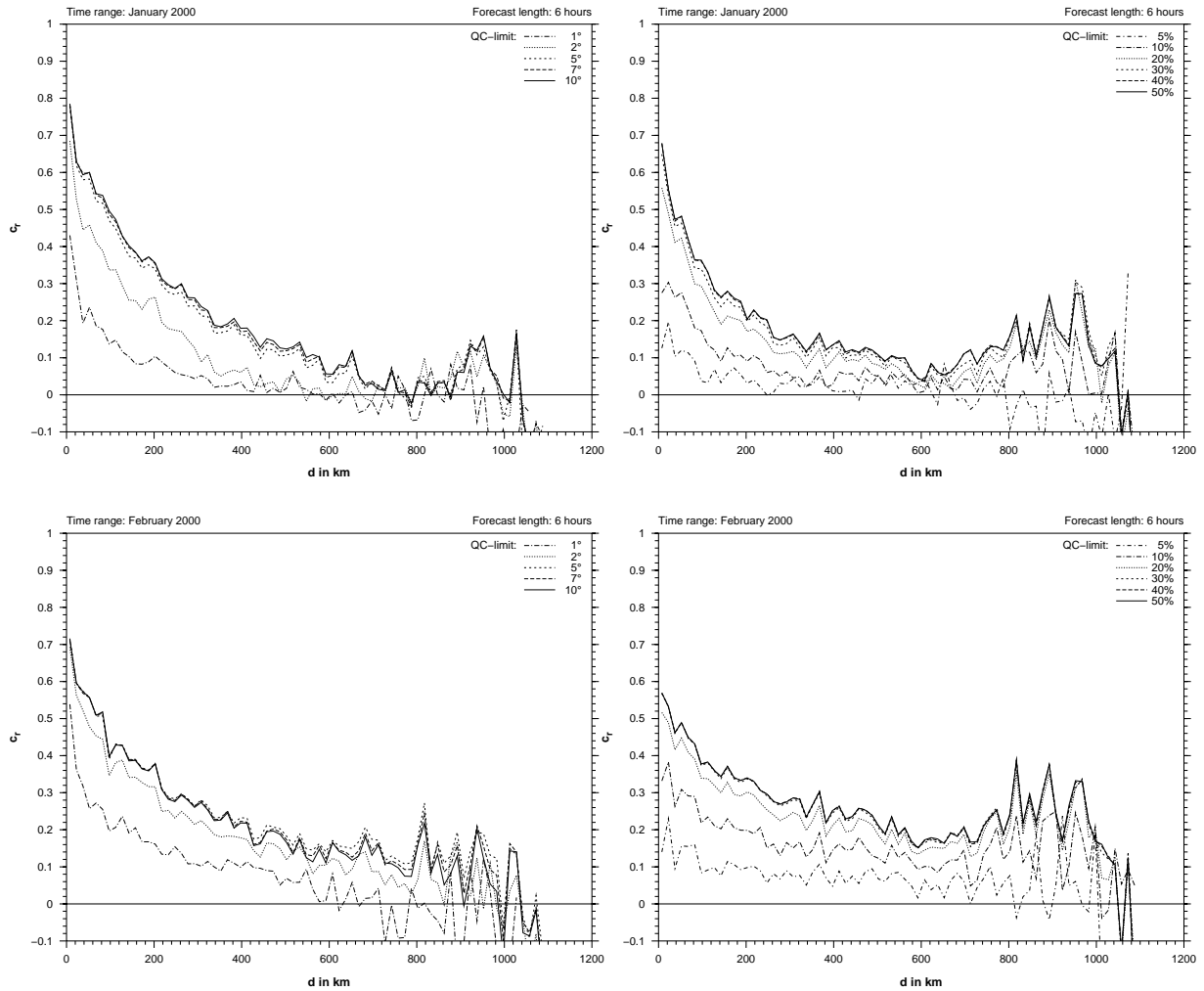


FIG. 4: Correlation of background minus observation in DMI-HIRLAM-D for T2m (left) and RH2m (right), valid for January (upper) and February (lower) respectively. The correlations are determined with 6 different quality control limits.

This effect also occurs in the medium resolution model (figure 3), and to a less extent in the high resolution model (figure 4).

It can be deduced from the curves that the correlation as a whole increases with growing quality control limit, even though the correlations for T2m from February show a slight maximum for the 5 K limit (figures 2, 3, 4 lower left respectively). The reason for this may be a growing number of errors occurring above 5 K, which have a random behaviour.

As a result from the above experiments, a limit of 5 K in T2m is chosen for the quality check. For RH2m, a limit of 30% seems appropriate for the further investigations.

### 3.3 Correlation fields

The assumption of isotropy as a major characteristic of the background error correlations is the basis for the methods described in sections 2.1 and 2.2. The validity of this assumption is investigated here. We make use of the NMC-Method in order to determine a horizontal field of the background

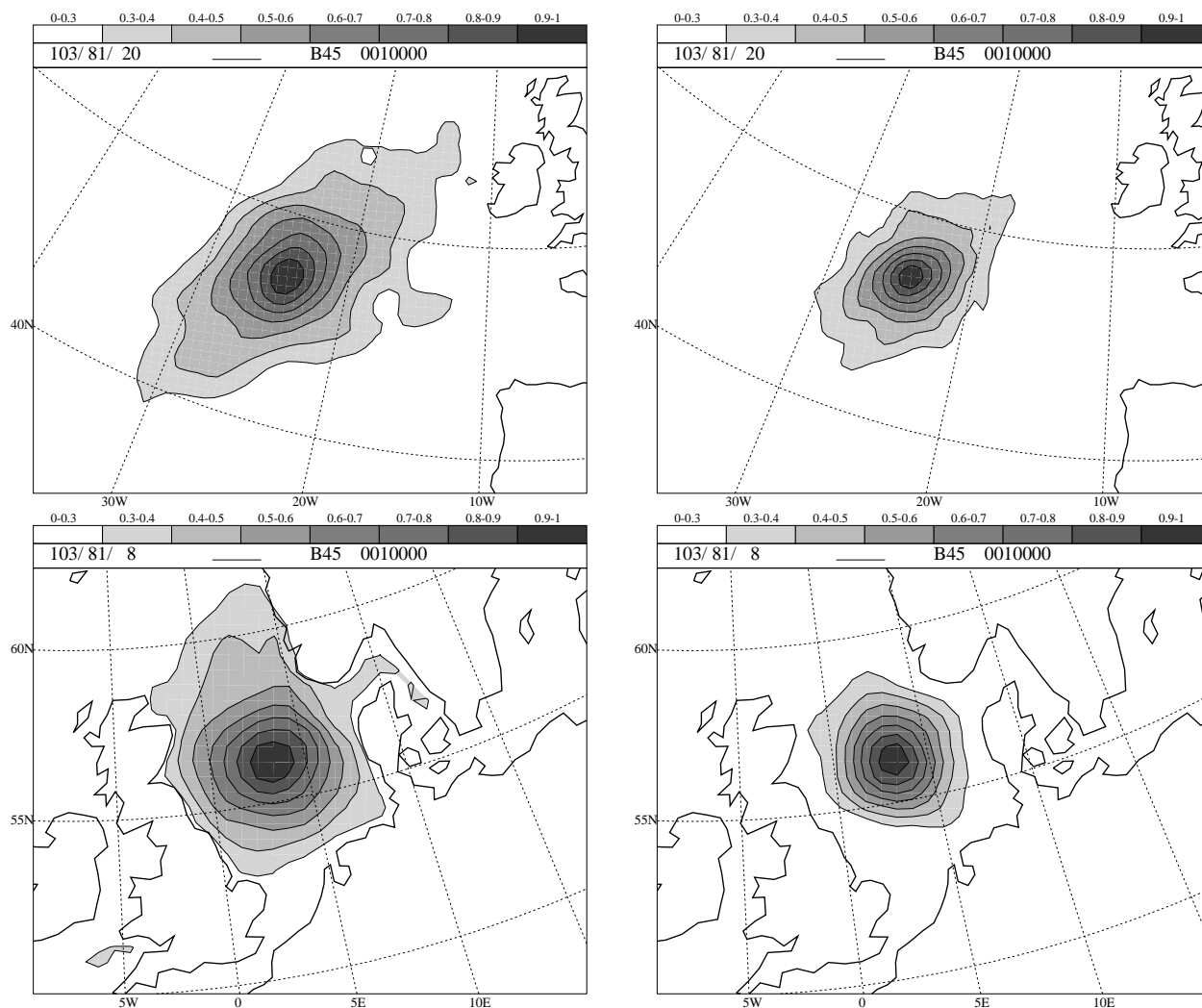


FIG. 5: Correlation fields for DMI-HIRLAM-G for T2m (figures to the left) and RH2m (figures to the right), determined with the NMC-Method with data from the period January to June 2000. The fields are related to a point over the North Atlantic (upper figures) and to a location in the North Sea (lower figures). See text for further details.

error correlation for selected points within the model domain. The data used for this investigation are taken from the operational forecasts of T2m and RH2m of DMI-HIRLAM-G and DMI-HIRLAM-D. The period is from January to June 2000.

The first location we consider is located over the North Atlantic at approximately  $32^{\circ}\text{W}$  and  $47^{\circ}\text{E}$  (figure 5 above). This point is far enough from the coast, thus avoiding possible influence from the land surface. It can be expected as a representative location for the North Atlantic area. In order to cover the surrounding area appropriately, data from DMI-HIRLAM-G are used. Both the background error correlation for T2m and for RH2m show a similar elliptic structure, with the major principal axes oriented SW-NE. It indicates the major flow direction, where relatively strong advective transport of field properties, including errors, takes place. The assumption of isotropy in background error correlation seems a rather crude approximation for this location.

Another selected point is located over the North Sea (the lower part of figure 5). The correlation distribution is almost symmetric for this location, indicating that the isotropic assumption is reason-

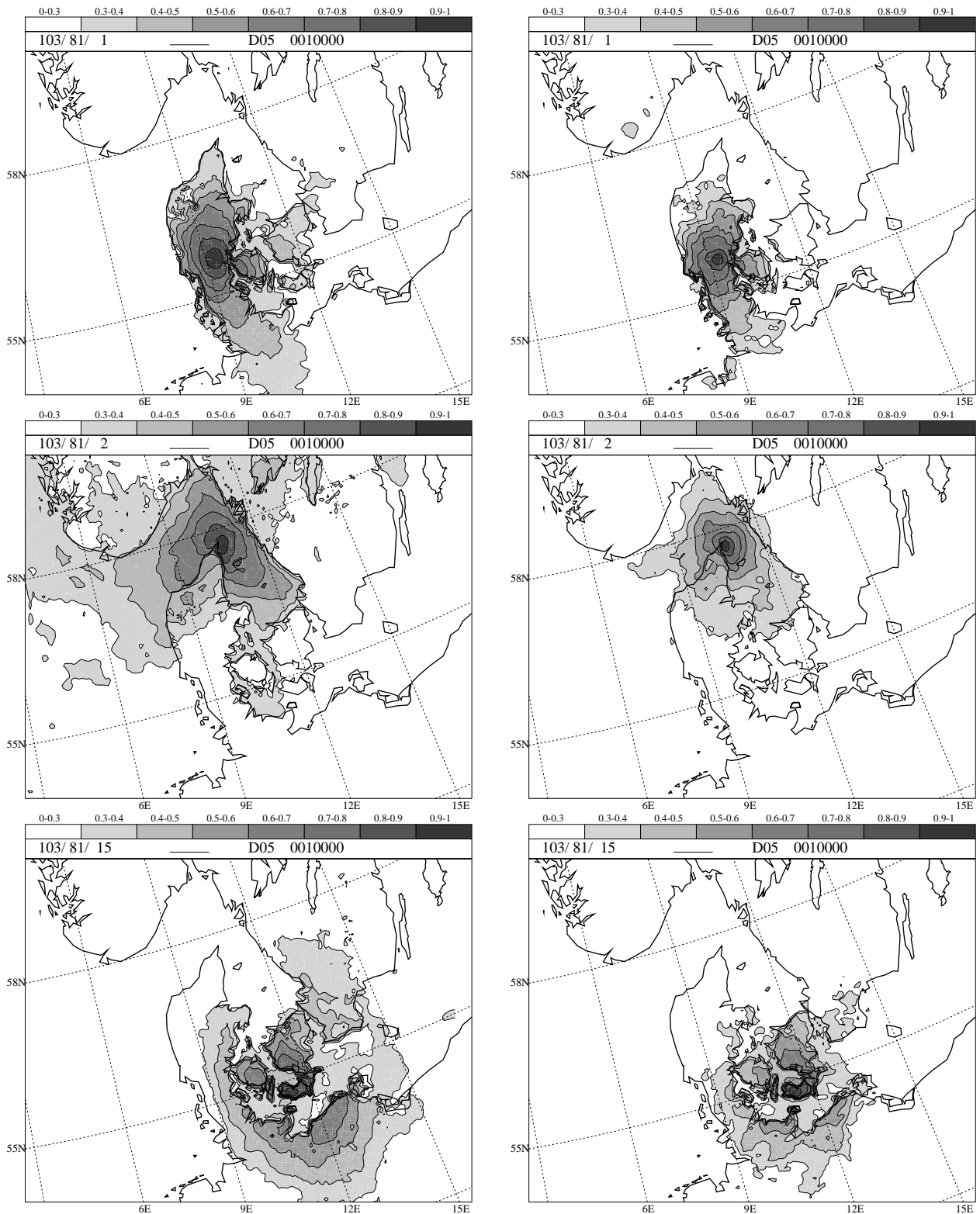


FIG. 6: Correlation fields of forecast error of DMI-HIRLAM-D, determined with the NMC-Method with data from the period January to June 2000, for T2m (figures to the left) and RH2m (figures to the right). The upper figures show the fields relative to a point in the middle of Jutland (Bilund), the middle figures are related to a coastal point (Skagen) and the fields in the lower figures refer to an island (Lolland).

able here. However, the influence of the land surface can be clearly recognized, at least for T2m, for which the spatial scale of correlation is large enough to reach the coastal areas.

It can be expected that grid representations of higher resolutions than  $0.45^\circ$  lead to very similar results over the sea, as other model properties remain unchanged, and grid resolution is not expected to change the isotropic properties of the background error correlations.

Figure 6 shows the correlation fields for the background error of T2m and RH2m in DMI-HIRLAM-D for three locations in Denmark. They represent an inland location (Bilund), a coastal point (Skagen) and an island (Lolland) respectively. The basic isotropic structure can be recognized in all three cases, although the influence of the land–sea contrast on the correlation structure is illuminating. The difference in correlation drops remarkably when the surface type changes between land and sea or vice versa.

Looking at the inland location Bilund, the correlation for T2m drops from 0.7 at the east coast of Jutland to approximately 0.45 over the sea, and increases again up to 0.7 over Fyn (figure 6 upper left). The same behaviour occurs for RH2m, where the correlation drops from values of about 0.6 to 0.3 at Jutland east coast and increases to almost 0.6 again over Fyn (figure 6 upper right).

A similar behaviour is found for the correlation field referring to Skagen, but just vice versa (figure 6 in the middle). The correlation drops significantly, as soon as the Swedish and the Norwegian coast are reached. It is interesting to see in the case of T2m some correlation in background error between the sea (Kattegat) and the Swedish lake Vännern (figure 6 middle to the right), indicating their similar treatment within the surface model of DMI-HIRLAM-D.

The most interesting structure of background error correlation shows for the island Lolland. In both T2m and RH2m, a sharp correlation drop occurs all around the islands' coast. At the northern coast, it is from 0.8 down to 0.5 for T2m (figure 6 lower to the left), and from 0.8 to 0.6 for RH2m (figure 6 lower to the right). The drop is even stronger at the southern coast, where the correlation decreases about 50% over the sea with respect to the land. As soon as the coast of Fyn, Jutland or Northern Germany is reached, the correlation becomes stronger with values over 0.6 for T2m and about 0.5 for RH2m.

The above investigations confirm that the assumption of isotropic structure functions for T2m and RH2m is a reasonable approximation for the background error correlations. It is valid regardless of the grid resolution of the model. The dependency of the structure function from the land–sea distribution is obvious and confirms the results of previous works (Gustafsson 1985 and Häggmark et al. 2000). It can be estimated from the figures that a correlation drop of up to 50% can occur in the surface representation of DMI-HIRLAM-D. The correlation fields already indicate different horizontal scales of correlation for T2m and RH2m, where the latter is smaller than the former. This difference will be discussed in more detail in the sections below.

### 3.4 Isotropic correlation curves

The correlation relations are investigated for the three different models DMI-HIRLAM-G, DMI-HIRLAM-E and DMI-HIRLAM-D within this section. The dependencies on surface properties and the monthly changes of the correlations are examined in the following sub-sections. An estimation on correlation scales is attempted at the end of this section.

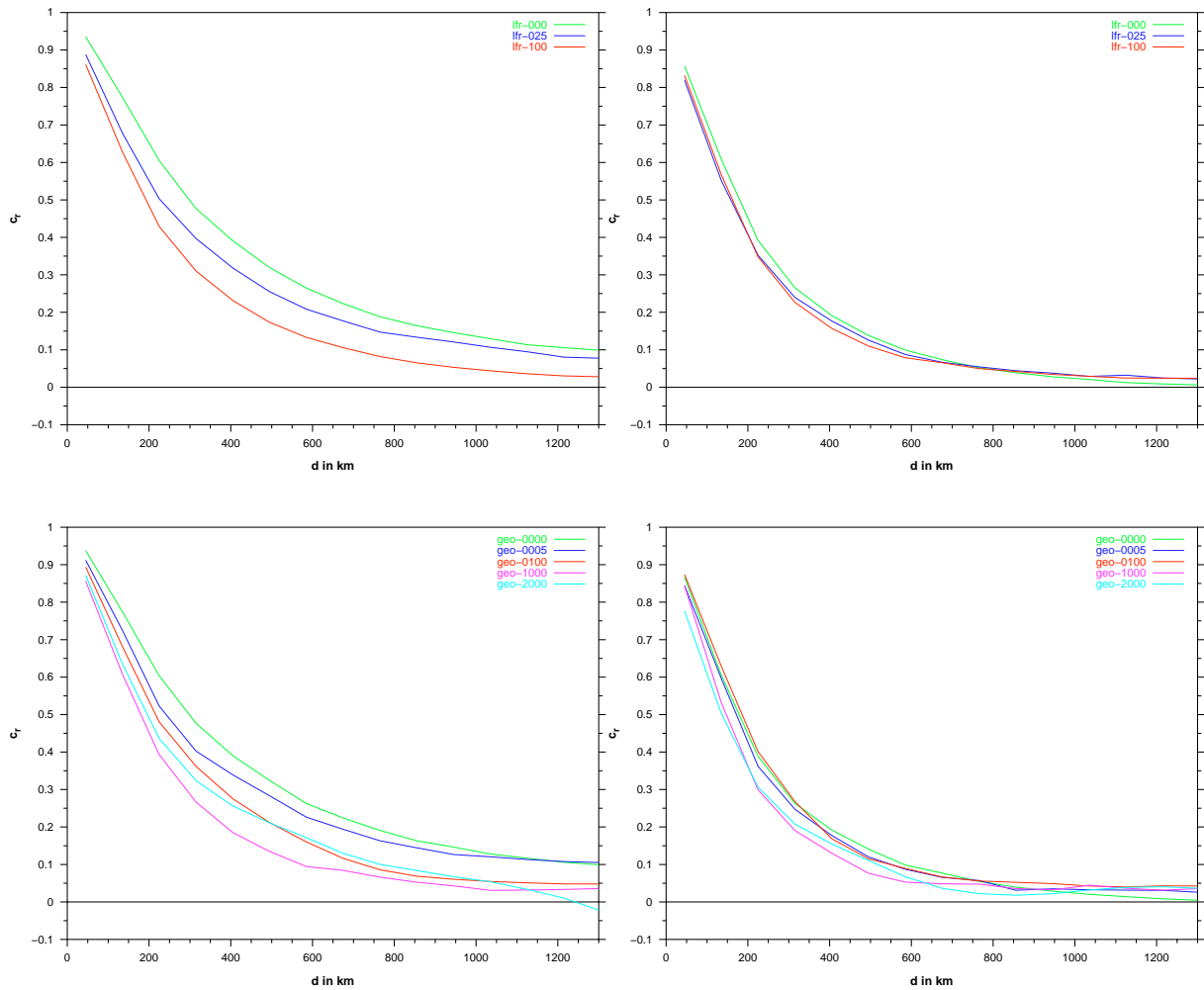


FIG. 7: Correlation in DMI-HIRLAM-G for the land fraction classes (upper figures) and the elevation classes (lower figures), as described in table 1, valid for T2m (left) and RH2m (right). The curves are based on data from the time range March 1st – May 31st, 2000.

### 3.4.1 Surface dependencies

As the model includes a different treatment of the surface over land and over sea, this has an influence on the background error correlations of near surface parameters. In order to investigate this, correlations are determined over areas with different land fraction using the NMC-Method. Three classes of this kind are identified. They are shown in table 1.

An additional investigation is performed by separation of points with different elevation. Five classes are identified, of which some can be considered to correspond with the classes separated with the help of the land fraction criteria (table 1).

The correlations are calculated from operational forecast data between March and May 2000. This time interval is assumed to be large enough to be representative and to show the important differences between the different surfaces.

Looking at the results for DMI-HIRLAM-G in figure 7, we can deduce that for T2m the background er-

ror correlations decrease significantly over land in comparison with sea (curves lfr-000 and lfr-100, as well as geo-0000 and geo-0100 at the left-hand side respectively). This is also true for DMI-HIRLAM-E (figure 8), but the correlations from DMI-HIRLAM-D do not show this difference (figure 9). The situation is different for relative humidity (see right-hand side of the figures 7 – 9). The correlations from DMI-HIRLAM-G show a slight decrease over land for RH2m, but only when regarding the curves determined with the land fraction criterion. The correlations from DMI-HIRLAM-E and DMI-HIRLAM-D tend to higher values over land for RH2m, especially with growing distance. (figures 8) and 9, right-hand side). For both T2m and RH2m can generally be stated the tendency towards less correlation when increasing the horizontal grid resolution of the model.

TAB. 1: Classes chosen for investigating the impact of surface properties on the background error correlations.

| Abbreviation | Criterion                               | Description            |
|--------------|---|------------------------|
| lfr-000      | $f_l = 0$                               | sea                    |
| lfr-025      | $5\% \leq f_l \leq 25\%$                | coastal regions        |
| lfr-100      | $f_l = 100\%$                           | land                   |
| geo-0000     | $h \leq 0$                              | sea                    |
| geo-0005     | $0 < h \leq 0.5\text{m}$                | mainly coastal regions |
| geo-0100     | $80\text{m} \leq h \leq 120\text{m}$    | flat land              |
| geo-1000     | $1000\text{m} \leq h \leq 1100\text{m}$ | hilly regions          |
| geo-2000     | $h > 2000\text{m}$                      | mountainous regions    |

It is interesting to note that both the class separation of land fraction and the one for elevation reveal the same effect what the land-sea difference in correlation is concerned. The same consistency between the two class separation methods is found when comparing the correlations between coastal points (lfr-025 and geo-0005) with the other curves. Compared to the curves valid for sea (lfr-000 and geo-0000), the correlation decreases at the coast. This is most significant for DMI-HIRLAM-E.

A physical reason for the decrease in background error correlation of T2m near the coast and over land compared to the sea is probably that there are much more locally influenced processes due to the significant change of the surface properties than there are over sea. This is true for relative humidity only in the case of coast, and only in the correlations from the models with higher resolution.

If we take a look at 2 meter temperature and compare the respective correlation curves of the land fraction classes from the three models (figures 7 – 9, upper left-hand side respectively), we can see large variations from DMI-HIRLAM-G towards DMI-HIRLAM-D in the curve representing sea, whereas there is less difference between the curves for land. This effect also occurs in the correlation curves of the elevation classes (figures 7 – 9, lower left-hand side respectively). It is probably due to the fact that the three models have a different coverage of the seas in their domain. Especially DMI-HIRLAM-D covers only the North Sea and parts of the Baltic Sea, whereas DMI-HIRLAM-E and DMI-HIRLAM-G also cover the North Atlantic, where large scale synoptic processes are dominant in contrast to the

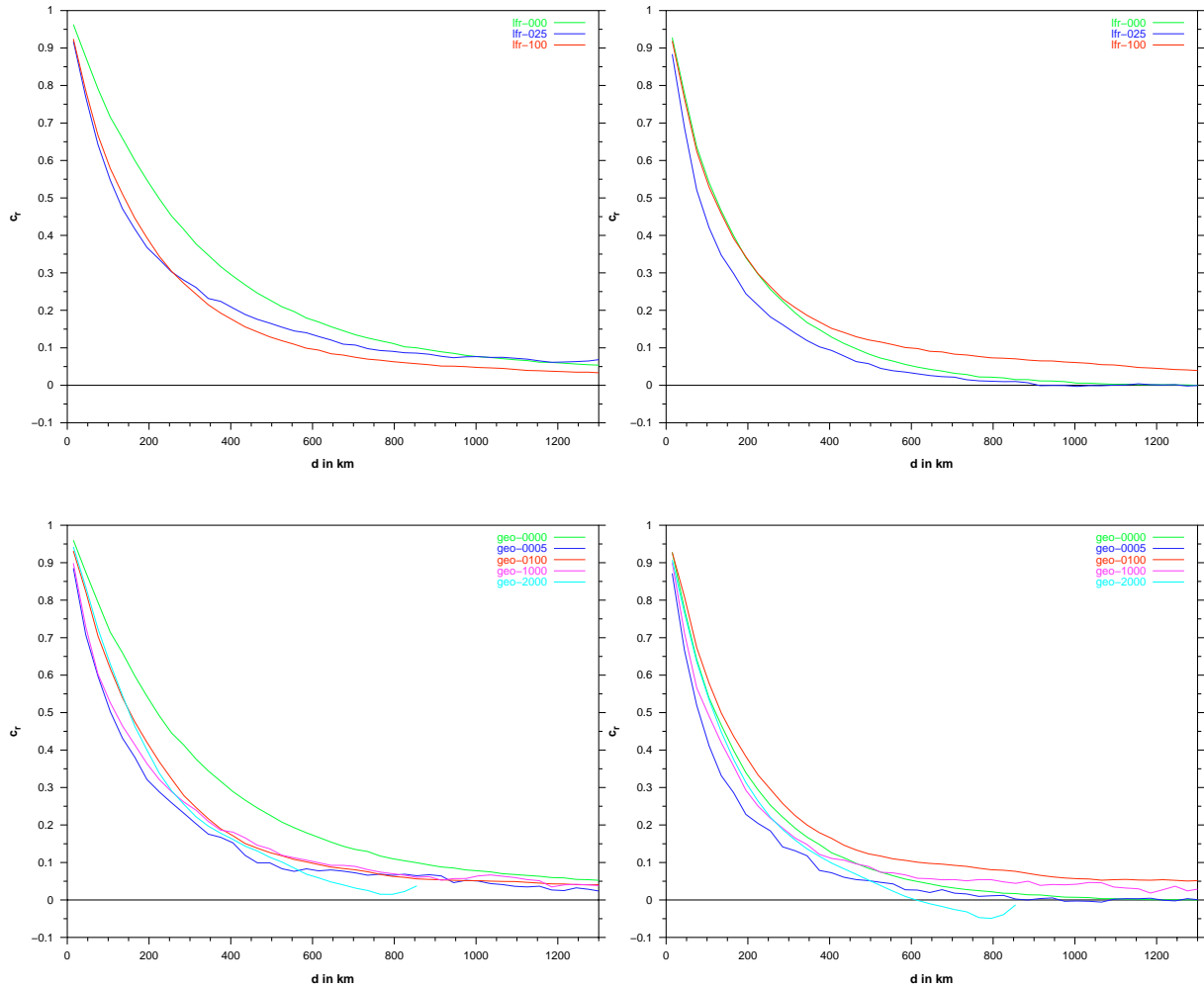


FIG. 8: Correlation in DMI-HIRLAM-E for the land fraction classes (upper figures) and the elevation classes (lower figures), as described in table 1, valid for T2m (left) and RH2m (right). The curves are based on data from the time range March 1st – May 31st, 2000.

North Sea and the Baltic Sea, which are influenced by local effects from the land.

The elevation classification includes further classes, which can be seen as representing hilly and mountainous regions (table 1). The background error correlations of points from these classes are also shown in figures 7, 8 and 9 for DMI-HIRLAM-G, DMI-HIRLAM-E and DMI-HIRLAM-D respectively. Looking at the class *hilly regions* (geo-1000), the tendency towards less correlation continues in comparison to *flat land* (geo-0100) and *sea* (geo-0000) for RH2m (lower right hand figures in figure 7, 8 and 9). The picture is more differentiated in T2m, where there seems to be a continued tendency towards increased correlation with growing elevation in DMI-HIRLAM-D, but not in DMI-HIRLAM-G (lower left-hand side figures in figures 7 – 9). There is however an uncertainty in these curves due to the limited number of points within the respective model domain, that were found to meet the class conditions, especially for DMI-HIRLAM-D.

The class *mountainous region* (geo-2000) could only be applied to the data from DMI-HIRLAM-G and DMI-HIRLAM-E, because DMI-HIRLAM-D does not contain enough such points. What the background error correlation in relative humidity is concerned, no significant changes in the correlations with

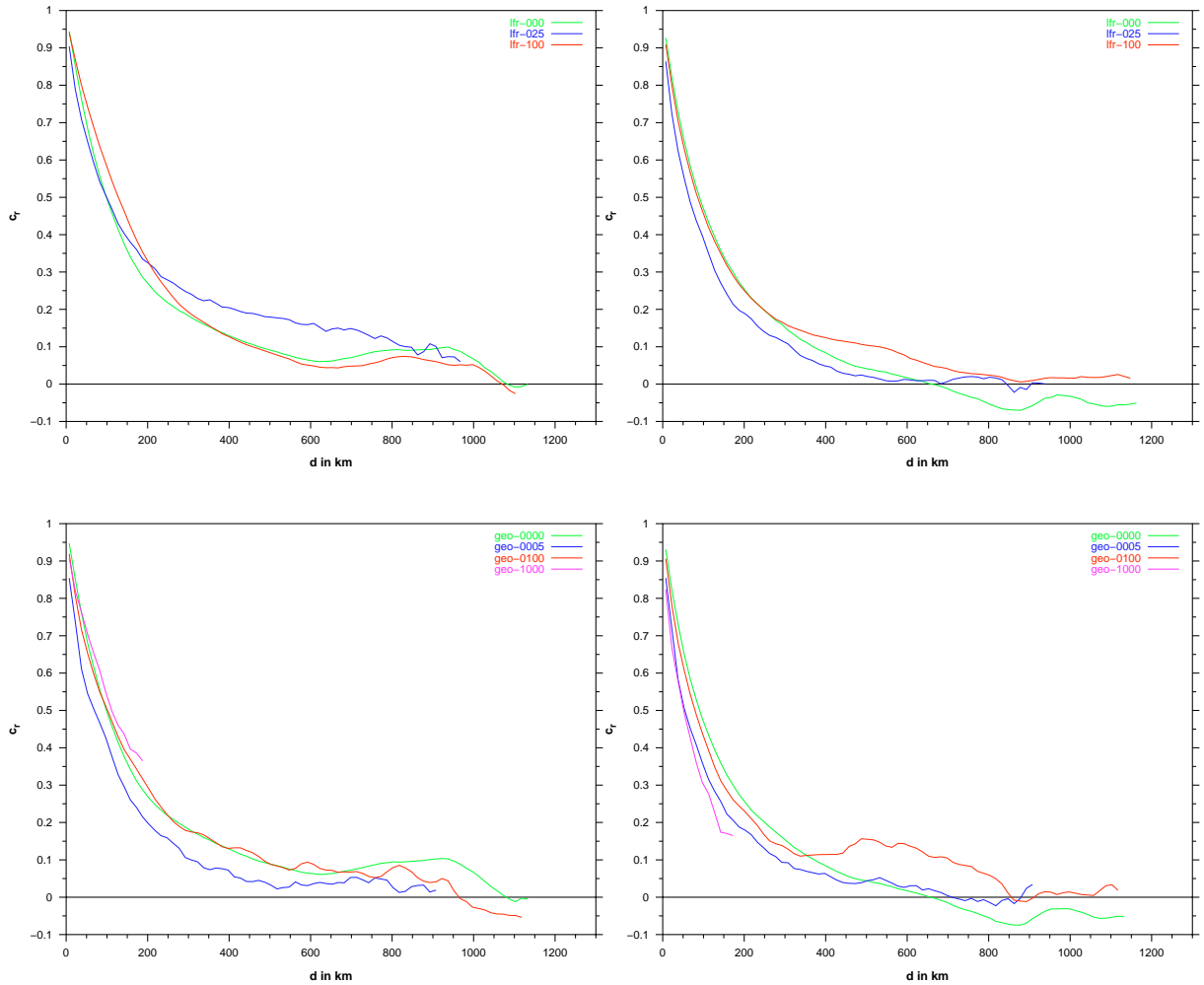


FIG. 9: Correlation in DMI-HIRLAM-D for the land fraction classes (upper figures) and the elevation classes (lower figures), as described in table 1, valid for T2m (left) and RH2m (right). The curves are based on data from the time range March 1st – May 31st, 2000.

respect to hilly terrain (geo-1000) are found, but there is a tendency towards more correlation in T2m, which may reflect the special treatment of the ABL in the models.

### 3.4.2 Comparison and monthly changes

The forecast error for a certain atmospheric parameter depends on the uncertainties arising from the differences in the model representation for different weather situations. It is obvious that the correlation of the background error thus changes with the synoptic pattern, and the forecast quality for a certain forecast length is not constant. It is therefore of interest to see the development of the correlation curves over a series months.

In order to make the curves from the Hollingsworth–Lönnerberg Method (HLM-curves) and those from the NMC–Method (NMC-curves) comparable, the HLM-curves are renormalized as described above (section 2.4). This also makes it possible to perform a comparison with the structure functions used in the surface analysis scheme of HIRLAM. The renormalization factor  $d_f$ , which is described

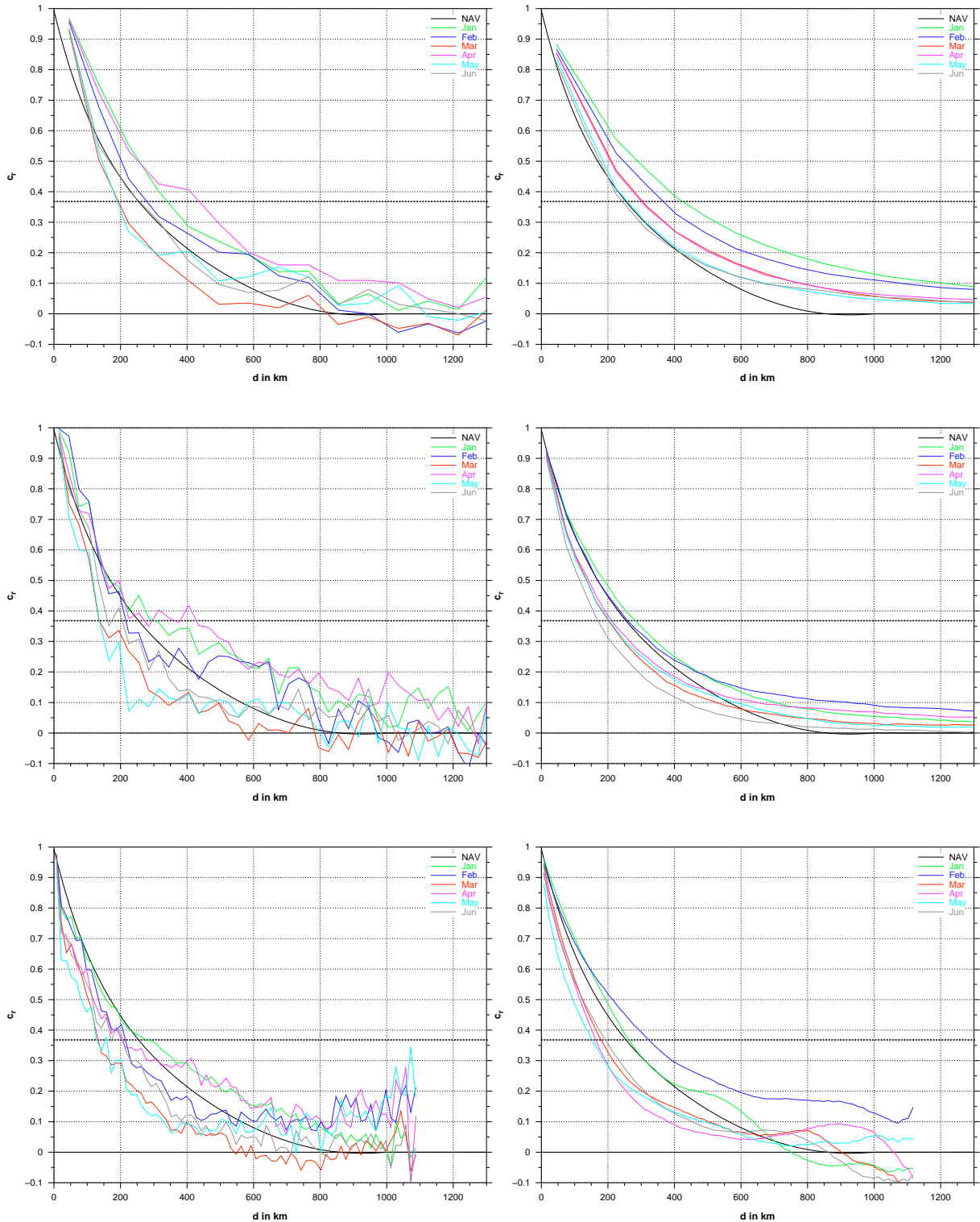


FIG. 10: Correlation curves in DMI-HIRLAM-G (upper), DMI-HIRLAM-E (middle) and DMI-HIRLAM-D (lower) for T2m, determined with the Hollingsworth–Lönnerberg Method (figures to the left) and the NMC–Method (figures to the right). Each curve represents a sample over one month. The thick solid curve (NAV) represents the function described by Navascues (1997), the horizontal dotted line depicts  $e^{-1}$ . See text for details.

in equation (16), was chosen to 180 km for the data from DMI-HIRLAM-G. This distance is a compromise between the demand to have enough data for the fitting process and the validity of the

fitting function, which is only fulfilled for small distances. The HLM-curves from DMI-HIRLAM-E and DMI-HIRLAM-D were renormalized in a similar way, where  $d_f$  was chosen to 60 km and 25 km, respectively.

As the observations used within the Hollingsworth–Lönnberg Method are actually all located over land, a corresponding criteria is applied in the NMC–Method in order to be consistent with the Hollingsworth–Lönnberg Method. The criteria for grid point separation within the NMC-calculations is based on land fraction and is chosen to  $f_l \geq 5\%$ .

#### I) MONTHLY CHANGES

Figures 10 and 11 show the correlation curves for the first six months of 2000 from the three operational models at DMI, for 2 meter temperature and relative humidity respectively. There is a clear variability from month to month in the correlations in all three models and for both parameters. Concerning T2m (figure 10), the variability in the HLM-curves is similar for all three models, whereas the NMC-curves show little less variability. The HLM-curves show a general decrease in correlation from January to March for T2m, high correlation in April and again lower values in May and June. The NMC-curves from DMI-HIRLAM-G for T2m clearly show a tendency towards less correlation between January and June (figure 10 upper to the right). This tendency is also found to a less extend in the curves from the other models.

The HLM-curves for RH2m have less variability than those for T2m and they have no obvious monthly trend. The NMC-curves from DMI-HIRLAM-G for RH2m indicate the monthly trend most clearly, with decreasing correlation values towards June, although the trend is weaker in the NMC-curves of DMI-HIRLAM-E and DMI-HIRLAM-D. It should be mentioned that there is a slight inhomogeneity in the data at the end of February 2000, which is due to changes in the operational set-up of the three models. However, higher correlations at the beginning of the year can still be recognized.

The irregular behaviour of the HLM-curves for large distances is connected with increased uncertainty, especially for the curves from DMI-HIRLAM-D. It should be noted that the size of the data sample becomes much smaller for the large distances, and the points lying close to the lateral border become dominant. The latter may explain the tendency towards increasing values of the correlations from DMI-HIRLAM-D at the largest possible distances due to the treatment of the lateral boundary.

#### II) COMPARISONS

The fitted functions for scaling the HLM-curves are not shown in the figures 10 and 11, because only the fitted value at  $d = 0$  is of interest (section 2.4). The figures include however the structure functions of the HIRLAM surface analysis for 2 meter temperature and relative humidity (Navascues 1997), which are described by

$$c_r(d) = \exp\left(\sum_{n=1}^6 a_n \left(\frac{d}{R}\right)^{n-1}\right) - 1, \quad (18)$$

where  $R = 1000$  km and the coefficients  $a_n$  as listed in table 2 are used (NAV-functions).

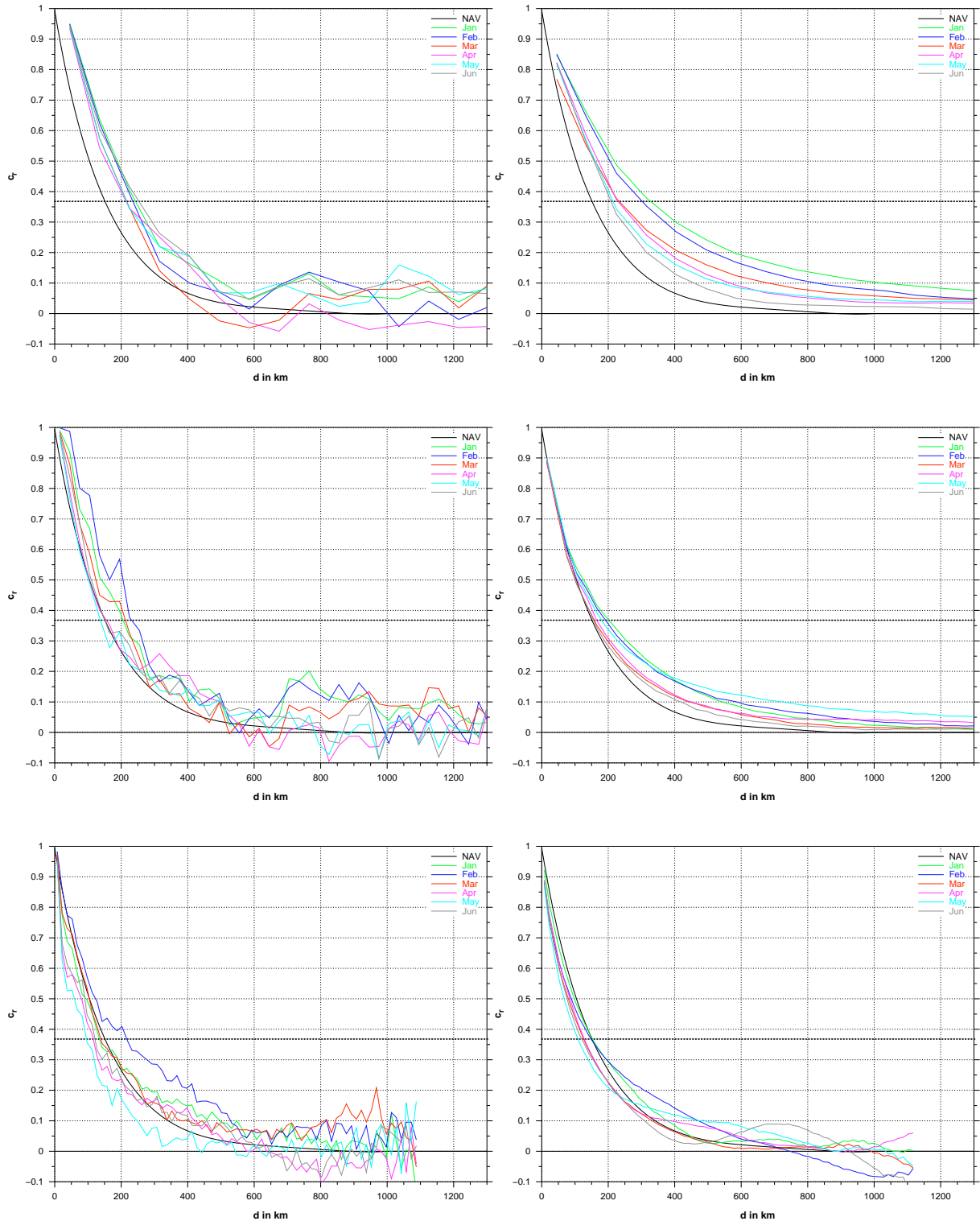


FIG. 11: Correlation curves in DMI-HIRLAM-G (upper), DMI-HIRLAM-E (middle) and DMI-HIRLAM-D (lower) for RH2m, determined with the Hollingsworth-Lönnberg Method (figures to the left) and the NMC-Method (figures to the right). Each curve represents a sample over one month. The thick solid curve (NAV) represents the function described by Navascues (1997), the horizontal dotted line depicts  $e^{-1}$ . For details see text.

One difference between the application of the Hollingsworth-Lönnberg Method and the NMC-Me-

thod is, that the number of points used for the correlation calculations usually is significantly higher in the latter. This is the reason for the NMC-curves behaving more smoothly than the HLM-curves.

TAB. 2: Coefficients used in the NAV-functions of equation (18).

| Parameter | $a_1$ | $a_2$ | $a_3$ | $a_4$ | $a_5$ | $a_6$ |
|-----------|-------|-------|-------|-------|-------|-------|
| T2m       | 0.69  | -2.27 | 4.43  | -6.43 | 5.11  | -1.53 |
| RH2m      | 0.69  | -3.30 | 5.98  | -4.37 | 0.47  | 0.53  |

As can be seen from the figures 10 and 11, the HLM-curves and the NMC-curves show a tendency towards smaller correlation values with increasing model resolution. This will be investigated quantitatively in the next sub-section.

The correspondence of both the HLM-curves and the NMC-curves to the NAV-functions is in general good for both T2m and RH2m. The curves from DMI-HIRLAM-G show larger correlations for a certain distance than the NAV-functions (figures 10 and 11 upper), while the curves from DMI-HIRLAM-D show lower correlation values (figures 10 and 11 lower). The correlations from DMI-HIRLAM-E are represented best by the NAV-functions (figures 10 and 11 middle).

The NMC-curves generally tend to have higher correlation values at large distances than the HLM-curves do. This becomes especially clear in the curves from DMI-HIRLAM-G and DMI-HIRLAM-E (figures 10 and 11 upper and middle right-hand side). This effect may reflect the special character of the NMC-Method that two forecast fields are correlated. Both fields are based on the model representation of the atmospheric equations and are based on the same approximations and parameterizations. These correlations remain even for large distances.

### 3.4.3 Scale estimations

We will now try to make an estimation for the correlation distance scales by determining the distance  $d$ , where  $c_r$  reaches a value of  $e^{-1}$ . This value is chosen, because the correlation curves behave like an e-function, and because the calculated curves do not descend clearly to zero at the large distances. Thus, the  $e^{-1}$ -value is regarded as to represent the main character of the curves best, what the distance scale is concerned.

The  $e^{-1}$ -distance is estimated for each parameter, model and method by determination of an average over the months. It is summarized in table 3. In the case of the NMC-curves for RH2m in DMI-HIRLAM-E, the curves for January and February were excluded because of their erroneous behaviour (figure 11 middle to right).

The tendency towards smaller distances with increasing model resolution is clearly pronounced in table 3 for both parameters and by both methods. The correspondence of the scales between the Hollingsworth-Lönnerberg Method and the NMC-Method is quite good, which indicates that the assumptions connected with the NMC-Method are permissible, and that the NMC-Method is a

TAB. 3: Estimation of the distances in km, from which the correlations are dropped down to by a factor of  $1/e$ . The estimations for the models are based on the respective averages over the monthly values, which are taken from the curves of figures 10 and 11. Further details are outlined in the text.

| Method                   | Parameter | DMI-HIRLAM-G | DMI-HIRLAM-E | DMI-HIRLAM-D |
|--------------------------|-----------|--------------|--------------|--------------|
| Lönnerberg–Hollingsworth | T2m       | 276          | 204          | 189          |
|                          | RH2m      | 232          | 182          | 137          |
| NMC                      | T2m       | 316          | 220          | 203          |
|                          | RH2m      | 250          | 177          | 131          |

sufficient alternative to the Hollingsworth–Lönnerberg Method. A closer look at the table reveals that the NMC-estimated scales are slightly larger than the corresponding HLM-estimated scales. This could be due to the linear assumption made in the NMC–Method. Due to this assumption, the error correlation scales are independent of forecast length. However, as pointed out by Bengtsson and Gustafsson (1971), this scale actually increases with forecast length. In this study, we use 36 hour and 12 hour forecasts to estimate background error with the NMC–Method, while 6 hour forecasts and observations are used with the Hollingsworth–Lönnerberg Method. Some corrections may be needed to account for the linear assumption when the NMC–Method is used.

Another reason for differences between the scales from the Hollingsworth–Lönnerberg Method and the NMC–Method is that the observation error  $\sigma_r$  is not a constant. Observations from coastal areas are for example less representative than observations from the interior, which increases  $\sigma_r$  for these observations. Including these observation in the Hollingsworth–Lönnerberg Method has an influence on the renormalization of the HLM-curves (section 2.4). It reduces the renormalization factors and thus the scales. However, an exclusion of all coastal observations, which make up 43% of the observations used in the Hollingsworth–Lönnerberg Method, would increase the uncertainty of the statistics in appropriately.

If we compare the scales from DMI-HIRLAM-G with those from DMI-HIRLAM-D, there is a reduction of about 30 % in the scale for T2m with respect to the low resolution model, regarding the values of the Hollingsworth–Lönnerberg Method (table 3). The reduction for RH2m is larger and approximately 40 %.

The reduction is not necessarily linear to the increase in horizontal grid resolution. Concerning T2m, the scale for the  $1/e$ -value changes much more between DMI-HIRLAM-G and DMI-HIRLAM-E than it does between DMI-HIRLAM-E and DMI-HIRLAM-D. Approximate proportional behaviour of the characteristic scale with respect to horizontal grid resolution is found, on the other hand, for RH2m. Depending on the parameter, horizontal grid resolution thus is not exclusively influencing the extend to which certain meteorological scales are represented in the model. Another important role may play the parameterization schemes used in the model. This will however not be followed up further in this report.

## 4 Comments on the current HIRLAM surface analysis scheme

Using the results presented in the previous sections, we now have a brief re-assessment on the study by Sattler et al. (2000). The following paragraphs will relate the first application of the HIRLAM surface analysis scheme at DMI, which was performed by Sattler et al. (2000), with respect to the structure function evaluations from above.

### 4.1 Error standard deviation

Within the work of Sattler et al. (2000), the following estimations for the error standard deviation were used:

| Parameter | Background | Observation |
|-----------|------------|-------------|
| T2m       | 2.0 K      | 0.5 K       |
| RH2m      | 22 %       | 10 %        |

The renormalization factors used in the analysis can be derived from equation (15). They are

$$\frac{\sigma_b^2}{\sigma_b^2 + \sigma_r^2} = 0.941 \text{ for T2m}$$

and

$$\frac{\sigma_b^2}{\sigma_b^2 + \sigma_r^2} = 0.829 \text{ for RH2m}$$

respectively. These values are significantly higher than the factors found during the scaling of the correlation curves from the Hollingsworth–Lönnberg Method in section 3.4.2, listed in table 4. They indicate that too large background errors were used by Sattler et al. (2000). Repeating the surface analysis with corrected background error standard deviation is recommended by the present study.

TAB. 4: Monthly renormalization factors for the correlation curves determined with the Hollingsworth–Lönnberg Method for T2m and RH2m, valid for DMI-HIRLAM-G, DMI-HIRLAM-E and DMI-HIRLAM-D. The rightmost column includes the values used by Sattler et al. (2000) for DMI-HIRLAM-D.

| Parameter | Model        | January | February | March | April | May   | June  | Applied |
|-----------|--------------|---------|----------|-------|-------|-------|-------|---------|
| T2m       | DMI-HIRLAM-G | 0.421   | 0.512    | 0.497 | 0.509 | 0.399 | 0.480 | –       |
|           | DMI-HIRLAM-E | 0.446   | 0.456    | 0.535 | 0.487 | 0.371 | 0.439 | –       |
|           | DMI-HIRLAM-D | 0.823   | 0.701    | 0.754 | 0.732 | 0.646 | 0.719 | 0.941   |
| RH2m      | DMI-HIRLAM-G | 0.416   | 0.415    | 0.401 | 0.403 | 0.352 | 0.388 | –       |
|           | DMI-HIRLAM-E | 0.456   | 0.435    | 0.471 | 0.438 | 0.418 | 0.376 | –       |
|           | DMI-HIRLAM-D | 0.765   | 0.664    | 0.661 | 0.692 | 0.636 | 0.708 | 0.829   |

It should be noted, however, that the calculations of the renormalization factors are based on correlations, which include observations from coastal areas. As mentioned in the previous section,  $\sigma_r$  is larger for such observations than it is for inland observations. Thus it can be expected that the renormalization factors become larger when applying the Hollingsworth–Lönnerberg Method by using only observations from the interior. An experiment, where all coastal observations (about 43% of the observations) were excluded really confirms this for DMI-HIRLAM-G and DMI-HIRLAM-E (table 5). It was not possible to show the effect for DMI-HIRLAM-D, because the number of remaining observations was too little in order to assure a useful statistics.

TAB. 5: Same as in table 4 for DMI-HIRLAM-G and DMI-HIRLAM-E, but with coastal observations excluded when applying the Hollingsworth–Lönnerberg Method. Values for DMI-HIRLAM-D are not shown, because there are not enough remaining observations in order to represent a good statistics.

| Parameter | Model        | January | February | March | April | May   | June  |
|-----------|--------------|---------|----------|-------|-------|-------|-------|
| T2m       | DMI-HIRLAM-G | 0.713   | 0.676    | 0.671 | 0.640 | 0.594 | 0.671 |
|           | DMI-HIRLAM-E | 0.694   | 0.653    | 0.705 | 0.709 | 0.696 | 0.593 |
| RH2m      | DMI-HIRLAM-G | 0.599   | 0.543    | 0.549 | 0.567 | 0.532 | 0.591 |
|           | DMI-HIRLAM-E | 0.598   | 0.572    | 0.547 | 0.553 | 0.539 | 0.550 |

## 4.2 Correlation scale

Another comparison concerns the distance scale of the correlation curves. The correlation parameterizations used in the surface analysis scheme (equation (18)) are plotted together with the correlation curves in figures 10 and 11. The  $e^{-1}$ -distance calculates to 254 km for T2m and 151 km for RH2m. Comparing this with the values from the Hollingsworth–Lönnerberg Method shown in table 3, we can see that the value for T2m lies between the scale of DMI-HIRLAM-G and DMI-HIRLAM-E, closest to DMI-HIRLAM-G. The value for RH2m is between DMI-HIRLAM-E and DMI-HIRLAM-D, where closer to the scale of DMI-HIRLAM-D. This conflicts with the speculation of Sattler et al. (2000) that the rather poor analysis of especially RH2m for cases dominated by local effects is due to the structure functions being only valid for larger scales. There are, however, two points which must be taken into account: Firstly, the time intervals do not coincide. Sattler et al. (2000) applied the analysis from the end of April to the middle of August. A comparison should be made at a later stage when data from the summer months are available. Secondly, the surface analysis scheme makes use of the box method (Lorenz 1981), which determines several analysis increments for a certain point. These values are combined in an averaging process (Källén 1996) and may have a smoothing effect on the analysis field.

## 5 Conclusions

The above results suggest an adaptation of the isotropic structure function for both 2 meter temperature and relative humidity when increasing the horizontal grid resolution of the background fields. Regarding the increase in resolution from  $0.45^\circ$  to  $0.05^\circ$  in DMI-HIRLAM, this adaptation should result in a reduction of the characteristic distance scale by approximately 30% in the case of 2 meter temperature, and approximately 40% in the case of 2 meter relative humidity. It is important to note that the reduction is not necessarily proportional to the increase in horizontal grid resolution. The relations depend on the regarded parameter.

The structure functions for 2 meter temperature and relative humidity depend on surface properties like land–sea contrast and elevation. There is a tendency towards less correlation over land for 2 meter temperature and for both parameters at the coast, which is due to the enhanced presence of local effects induced by strong surface contrasts. The significant drop in background error correlation at coastal areas indicates the importance of including a different treatment of such areas within a surface analysis scheme.

The results indicate that the NMC–Method is an appropriate alternative to the Hollingsworth–Lönnberg Method, which means that observation data can be avoided when determining isotropic structure functions. However, minor corrections in the obtained correlation scales may be needed. The results also suggest a decrease in the correlations towards summer time. Seasonal changes should be taken into account by the surface analysis in the future.

Concerning the HIRLAM surface analysis scheme, it is possible to apply it on high resolution background data like from DMI-HIRLAM-D, the structure functions should, however, be adapted. A further investigation of the HIRLAM surface analysis scheme is in this connection desirable. It would also be of interest, how the structure functions for other parameters behave when increasing the horizontal resolution of the background fields.

## Acknowledgments

We like to thank Bjarne Amstrup for providing tools to extract observation data from DMIs BUFR archives. He provided also the chart of Figure 1. Furthermore are we very grateful to Nils Gustafsson for his fruitful comments.

## A List of Symbols

|                            |  |
|----------------------------|--|
| $b_{ij}$                   | background error covariance between point $i$ and $j$              |
| $c_r$                      | correlation in general   |
| $c_{r,l}$                  | correlation of background – observation (Hollingsworth–Lönnerberg) |
| $c_{r,n}$                  | correlation of 12h – 36h forecasts (NMC–Method)                    |
| $c_{r,s}$                  | $c_{r,l}$ scaled   |
| $d$                        | distance   |
| $h$                        | elevation height   |
| $i, j$                     | indices of a grid point or observation location                    |
| $L$                        | Length scale   |
| $f_l$                      | land fraction  |
| $r_{ij}$                   | observation error covariance between point $i$ and $j$             |
| $s_{ij}$                   | sum of $b_{ij}^{6h}$ and $r_{ij}$                                  |
| $x^{b6}, x^{b12}, x^{b36}$ | background value from 6h, 12h and 36h respectively                 |
| $x_{corr}^{b6}$            | background value with bias correction                              |
| $x^r$                      | observed value   |
| $x^t$                      | true value   |
| $\Delta x_{max}$           | quality control limit  |
| $\sigma_b$                 | background error   |
| $\sigma_r$                 | observation error  |

## References

- Bengtsson, L. and Gustafsson, N., 1971: An experiment in the assimilation of data in dynamical analysis. *Tellus*, **23**, 328–336.
- Daley, R., 1991: Atmospheric Data Analysis. *Cambridge University Press*. ISBN 0-521-38215-7.
- Gandin, L.S., 1963: Objective analysis of meteorological fields. *Translated from Russian by the Israeli Program for Scientific Translations, 1965*, 242 pp.
- Garçia–Moya, J.A., P del Río, Calvo, J., Nvascues, B., Esteban, L., Calvo, M., 2000: The new operational Hirlam at INM. *Hirlam Newsletter*, **35**, 59–66.
- Gustafsson, N., 1985: Development of Meso-Scale Analysis Schemes for Nowcasting and very high Short-Range Forecasting. *Proceedings from Workshop on High Resolution Analysis*, ECMWF, UK, 183–212.
- Häggmark, L., Ivarsson, K.-I., Gollvik, S., Olofsson, P.-O., 2000: Mesan, an operational mesoscale analysis system. *Tellus*, **52A**, 2–20.
- Hollingsworth, A., Lönnberg, P., 1986: The statistical structure of short-range forecast errors as determined from radiosonde data. Part I.: The wind field. *Tellus*, **38A**, 111–136.
- Källén, E. (ed.), 1996: HIRLAM Documentation Manual system 2.5.
- Lorenc, A.C., 1981: A Global Three-Dimensional Multivariate Statistical Interpolation Scheme. *Mon. Wea. Rev.*, **109**, 701–721.
- Lönnberg, P., Hollingsworth, A., 1986: The statistical structure of short-range forecast errors as determined from radiosonde data. Part II.: The covariance of height and wind errors. *Tellus*, **38A**, 137–161.
- Navascues, B., 1997: Analysis of 2 meter Temperature and Relative Humidity. *Hirlam Tech. Rep.*, **28**.
- Parrish, D.F., Derber, J.C., 1992: The National Meteorological Centre's Statistical Interpolation Analysis System. *Mon. Wea. Rev.*, **120**, 1747–1763.
- Puri, K., Lönnberg, P., 1991: Use of High-Resolution Structure Functions and Modified Quality Control in the Analysis of Tropical Cyclones. *Mon. Wea. Rev.*, **119**, 1151–1167.
- Rabier, F., McNally, A., Andersson, E., Courtier, P., Eyre, J., Hollingsworth, A. and Bouttier, F., 1998: The ECMWF implementation of three dimensional variational assimilation (3D-Var). Part II: Structure functions. *Quart. J. Roy. Meteor. Soc.*, **124**, 1809–1830.
- Rodríguez, E., 2000: personal communication.
- Sass, B.H., Nielsen, N.W., Jørgensen, J.U., Amstrup, B., 1999: The operational HIRLAM system at DMI – October 1999 –. *DMI Tech. Rep.*, **99-21**.

Sattler, K., Amstrup, B., Hilden, A., Hansen, J., 2000: Evaluation of the HIRLAM Surface Analysis Scheme for 2 meter Temperature and Relative Humidity by Comparison with AMIS gridded Observations. *DMI Tech. Rep.*, **00-09**.

# DANISH METEOROLOGICAL INSTITUTE

## Scientific Reports

Scientific reports from the Danish Meteorological Institute cover a variety of geophysical fields, i.e. meteorology (including climatology), oceanography, subjects on air and sea pollution, geomagnetism, solar-terrestrial physics, and physics of the middle and upper atmosphere.

Reports in the series within the last five years:

No. 95-1

**Peter Stauning** and T.J. Rosenberg:  
High-Latitude, day-time absorption spike events  
1. morphology and occurrence statistics  
Not published

No. 95-2

**Niels Larsen**: Modelling of changes in stratospheric ozone and other trace gases due to the emission changes : CEC Environment Program Contract No. EV5V-CT92-0079. Contribution to the final report

No. 95-3

**Niels Larsen, Bjørn Knudsen, Paul Eriksen, Ib Steen Mikkelsen, Signe Bech Andersen and Torben Stockflet Jørgensen**: Investigations of ozone, aerosols, and clouds in the arctic stratosphere : CEC Environment Program Contract No. EV5V-CT92-0074. Contribution to the final report

No. 95-4

**Per Høeg and Stig Syndergaard**: Study of the derivation of atmospheric properties using radio-occultation technique

No. 95-5

Xiao-Ding Yu, **Xiang-Yu Huang** and **Leif Laurssen** and Erik Rasmussen: Application of the HIRLAM system in China: heavy rain forecast experiments in Yangtze River Region

No. 95-6

**Bent Hansen Sass**: A numerical forecasting system for the prediction of slippery roads

No. 95-7

**Per Høeg**: Proceeding of URSI International Conference, Working Group AFG1 Copenhagen, June 1995. Atmospheric research and applications using observations based on the GPS/GLONASS System  
Not published

No. 95-8

**Julie D. Pietrzak**: A comparison of advection schemes for ocean modelling

No. 96-1

**Poul Frich** (co-ordinator), H. Alexandersson, J. Ashcroft, B. Dahlström, G.R. Demarée, A. Drebs, A.F.V. van Engelen, E.J. Førland, I. Hanssen-Bauer, R. Heino, T. Jónsson, K. Jonasson, L. Keegan, P.Ø. Nordli, **T. Schmith, P. Steffensen**, H. Tuomenvirta, O.E. Tveito: North Atlantic Climatological Dataset (NACD Version 1) - Final report

No. 96-2

**Georg Kjærgaard Andreassen**: Daily response of high-latitude current systems to solar wind variations: application of robust multiple regression. Methods on Godhavn magnetometer data

No. 96-3

**Jacob Woge Nielsen, Karsten Bolding Kristensen, Lonny Hansen**: Extreme sea level highs: a statistical tide gauge data study

No. 96-4

**Jens Hesselbjerg Christensen, Ole Bøssing Christensen, Philippe Lopez**, Erik van Meijgaard, Michael Botzet: The HIRLAM4 Regional Atmospheric Climate Model

No. 96-5

**Xiang-Yu Huang**: Horizontal diffusion and filtering in a mesoscale numerical weather prediction model

No. 96-6

**Henrik Svensmark and Eigil Friis-Christensen**: Variation of cosmic ray flux and global cloud coverage - a missing link in solar-climate relationships

No. 96-7

**Jens Havskov Sørensen and Christian Ødum Jensen**: A computer system for the management of epidemiological data and prediction of risk and economic consequences during outbreaks of foot-and-mouth disease. CEC AIR Programme. Contract No. AIR3 - CT92-0652

No. 96-8

**Jens Havskov Sørensen**: Quasi-automatic of input for LINCOM and RIMPUFF, and output conversi-

on. CEC AIR Programme. Contract No. AIR3 - CT92-0652

No. 96-9

**Rashpal S. Gill and Hans H. Valeur:**

Evaluation of the radarsat imagery for the operational mapping of sea ice around Greenland

No. 96-10

**Jens Hesselbjerg Christensen,** Bennert Machenhauer, Richard G. Jones, Christoph Schär, Paolo Michele Ruti, Manuel Castro and Guido Visconti: Validation of present-day regional climate simulations over Europe: LAM simulations with observed boundary conditions

No. 96-11

**Niels Larsen, Bjørn Knudsen, Paul Eriksen, Ib Steen Mikkelsen, Signe Bech Andersen and Torben Stockflet Jørgensen:** European Stratospheric Monitoring Stations in the Arctic: An European contribution to the Network for Detection of Stratospheric Change (NDSC): CEC Environment Programme Contract EV5V-CT93-0333: DMI contribution to the final report

No. 96-12

**Niels Larsen:** Effects of heterogeneous chemistry on the composition of the stratosphere: CEC Environment Programme Contract EV5V-CT93-0349: DMI contribution to the final report

No. 97-1

**E. Friis Christensen og C. Skøtt:** Contributions from the International Science Team. The Ørsted Mission - a pre-launch compendium

No. 97-2

**Alix Rasmussen, Sissi Kiilsholm, Jens Havskov Sørensen, Ib Steen Mikkelsen:** Analysis of tropospheric ozone measurements in Greenland: Contract No. EV5V-CT93-0318 (DG 12 DTEE): DMI's contribution to CEC Final Report Arctic Tropospheric Ozone Chemistry ARCTOC

No. 97-3

**Peter Thejll:** A search for effects of external events on terrestrial atmospheric pressure: cosmic rays

No. 97-4

**Peter Thejll:** A search for effects of external events on terrestrial atmospheric pressure: sector boundary crossings

No. 97-5

**Knud Lassen:** Twentieth century retreat of sea-ice in the Greenland Sea

No. 98-1

**Niels Woetman Nielsen, Bjarne Amstrup, Jess U. Jørgensen:**

HIRLAM 2.5 parallel tests at DMI: sensitivity to type of schemes for turbulence, moist processes and advection

No. 98-2

**Per Høeg, Georg Bergeton Larsen, Hans-Henrik Benzou, Stig Syndergaard, Mette Dahl Mortensen:** The GPSOS project

Algorithm functional design and analysis of ionosphere, stratosphere and troposphere observations

No. 98-3

**Mette Dahl Mortensen, Per Høeg:**

Satellite atmosphere profiling retrieval in a nonlinear troposphere

Previously entitled: Limitations induced by Multipath

No. 98-4

**Mette Dahl Mortensen, Per Høeg:**

Resolution properties in atmospheric profiling with GPS

No. 98-5

**R.S. Gill and M. K. Rosengren**

Evaluation of the Radarsat imagery for the operational mapping of sea ice around Greenland in 1997

No. 98-6

**R.S. Gill, H.H. Valeur, P. Nielsen and K.Q. Hansen:** Using ERS SAR images in the operational mapping of sea ice in the Greenland waters: final report for ESA-ESRIN's: pilot projekt no. PP2.PP2.DK2 and 2<sup>nd</sup> announcement of opportunity for the exploitation of ERS data projekt No. AO2..DK 102

No. 98-7

**Per Høeg et al.:** GPS Atmosphere profiling methods and error assessments

No. 98-8

**H. Svensmark, N. Woetmann Nielsen and A.M. Sempreviva:** Large scale soft and hard turbulent states of the atmosphere

No. 98-9

**Philippe Lopez, Eigil Kaas and Annette Guldborg:** The full particle-in-cell advection scheme in spherical geometry

No. 98-10

**H. Svensmark:** Influence of cosmic rays on earth's climate

No. 98-11

**Peter Thejll and Henrik Svensmark:** Notes on the method of normalized multivariate regression

No. 98-12

**K. Lassen:** Extent of sea ice in the Greenland Sea 1877-1997: an extension of DMI Scientific Report 97-5

No. 98-13

**Niels Larsen, Alberto Adriani and Guido Di-Donfrancesco:** Microphysical analysis of polar stratospheric clouds observed by lidar at McMurdo, Antarctica

No.98-14

**Mette Dahl Mortensen:** The back-propagation method for inversion of radio occultation data

No. 98-15

**Xiang-Yu Huang:** Variational analysis using spatial filters

No. 99-1

**Henrik Feddersen:** Project on prediction of climate variations on seasonal to interannual time-scales (PROVOST) EU contract ENV4-CT95-0109: DMI contribution to the final report: Statistical analysis and post-processing of uncoupled PROVOST simulations

No. 99-2

**Wilhelm May:** A time-slice experiment with the ECHAM4 A-GCM at high resolution: the experimental design and the assessment of climate change as compared to a greenhouse gas experiment with ECHAM4/OPYC at low resolution

No. 99-3

**Niels Larsen et al.:** European stratospheric monitoring stations in the Arctic II: CEC Environment and Climate Programme Contract ENV4-CT95-0136. DMI Contributions to the project

No. 99-4

**Alexander Baklanov:** Parameterisation of the deposition processes and radioactive decay: a review and some preliminary results with the DERMA model

No. 99-5

**Mette Dahl Mortensen:** Non-linear high resolution inversion of radio occultation data

No. 99-6

**Stig Syndergaard:** Retrieval analysis and methodologies in atmospheric limb sounding using the GNSS radio occultation technique

No. 99-7

**Jun She, Jacob Woge Nielsen:** Operational wave forecasts over the Baltic and North Sea

No. 99-8

**Henrik Feddersen:** Monthly temperature forecasts for Denmark - statistical or dynamical?

No. 99-9

**P. Thejll, K. Lassen:** Solar forcing of the Northern hemisphere air temperature: new data

No. 99-10

**Torben Stockflet Jørgensen, Aksel Walløe Hansen:** Comment on "Variation of cosmic ray flux and global coverage - a missing link in solar-climate relationships" by Henrik Svensmark and Eigil Friis-Christensen

No. 99-11

**Mette Dahl Meincke:** Inversion methods for atmospheric profiling with GPS occultations

No. 99-12

**Benzon, Hans-Henrik; Olsen, Laust:** Simulations of current density measurements with a Faraday Current Meter and a magnetometer

No. 00-01

**Høeg, P.; Leppelmeier, G:** ACE: Atmosphere Climate Experiment: proposers of the mission

No. 00-02

**Høeg, P.:** FACE-IT: Field-Aligned Current Experiment in the Ionosphere and Thermosphere

No. 00-03

**Allan Gross:** Surface ozone and tropospheric chemistry with applications to regional air quality modeling. PhD thesis

No. 00-04

**Henrik Vedel:** Conversion of WGS84 geometric heights to NWP model HIRLAM geopotential heights

No. 00-05

**Jérôme Chenevez:** Advection experiments with DMI-Hirlam-Tracer

No. 00-06

**Niels Larsen:** Polar stratospheric clouds microphysical and optical models

No. 00-07

**Alix Rasmussen, Jens Havskov Sørensen, Niels Woetmann Nielsen, Bjarne Amstrup:** Uncertainty of meteorological parameters from DMI-HIRLAM

No. 00-08

**A.L. Morozova:** Solar activity and Earth's weather. Effect of the forced atmospheric transparency changes on the troposphere temperature profile studied with atmospheric models

No. 00-09

**Niels Larsen, Bjørn M. Knudsen, Michael Gauss, Giovanni Pitari:** Effects from high-speed civil traffic aircraft emissions on polar stratospheric clouds

No. 00-10

**Søren Andersen:** Evaluation of SSM/I sea ice algorithms for use in the SAF on ocean and sea ice, July 2000

No. 00-11

**Claus Petersen, Niels Woetmann Nielsen:** Diagnosis of visibility in DMI-HIRLAM

No. 00-12

**Erik Buch:** A monograph on the physical oceanography of the Greenland waters

No. 00-13

**M. Steffensen:** Stability indices as indicators of lightning and thunder

No. 00-14

**Bjarne Amstrup, Kristian S. Mogensen, Xiang-Yu Huang:** Use of GPS observations in an optimum interpolation based data assimilation system

No. 00-15

**Mads Hvid Nielsen:** Dynamisk beskrivelse og hydrografisk klassifikation af den jyske kyststrøm (In press)

No. 00-16

**Kristian S. Mogensen, Jess U. Jørgensen, Bjarne Amstrup, Xiaohua Yang and Xiang-Yu Huang:** Towards an operational implementation of HIRLAM 3D-VAR at DMI